

Shear wave noise attenuation and wavefield separation in curvelet domain

Chenhao Yang, Yi Huang, Zhaojun Liu, Jianming Sheng, Eric Camarda, TGS

Summary

One of the advantages of ocean bottom seismic data is combining hydrophone and vertical geophone data for ghost reflection attenuation. However, when the seafloor is rough and rugged, the scattered shear wave noise will contaminate the geophone data and strongly affect the image quality. The conventional workflow for wavefield separation includes applying shear wave denoise on geophone data first, then combining geophone and hydrophone data for P/Z matching and upgoing/downgoing wavefield separation. In this paper, we propose a new approach that can achieve denoising and matching simultaneously by local attribute matching in the curvelet domain. The proposed method makes use of local dip and scale information to conduct local attribute matching for noise suppression and P/Z matching. This method is applied to real dataset examples for validation. Results show that the new method can successfully suppress the noise with very limited signal leakage. Upgoing wavefield migration results are also provided to prove the P/Z matching was performed effectively. The image quality is significantly improved when compared with the original hydrophone migration image.

Introduction

Recently, Ocean Bottom Cable (OBC) and Ocean Bottom Node (OBN) technology have been widely used for high-quality seismic imaging. Both methods use hydrophones to record the pressure wavefield and geophones to record the 3-components elastic wavefield. These hydrophone and geophone data can be combined to achieve up/down separation, then up/down deconvolution can be performed for free surface multiple attenuation. However, up/down deconvolution is very sensitive to the data quality and signal to noise ratio. Therefore, noise attenuation is required before up/down deconvolution.

There are two main challenges exist in wavefield separation. First is the presence of strong shear wave noise in geophone data. The exact origin of this shear wave noise is still unknown; however, recent research suggests it comes from converted S-wave energy originating at near-surface scattering points (Paffenholz et al. 2006a, 2006b). When the sediment is rough and rugged, with complex seafloor structure, the shear wave noise will be even more severe. The second challenge is the hydrophone/geophone (P/Z) matching. Additional correction is needed when the hydrophone/geophone are not perfectly calibrated. Also,

geophone amplitude attenuation is incident-angle-dependent, while the hydrophone is not sensitive to the obliquity.

The conventional processing workflow includes two parts, first suppress the shear wave noise, then calibrate hydrophone/geophone and apply P/Z summation to generate the upgoing and downgoing wavefields. Previous methods for shear wave attenuation mainly focused on noise modeling and velocity filtering. Brittan and Starr (2003) used water layer reverberation models to separate the noise and signal. However, it requires 1-D approximation for the velocity model which is perhaps not suited for rough seafloors and complex subsurface structures. The difference will be further amplified as the incident angle increases.

F-K domain velocity filtering is another attempt for shear wave attenuation (Shatilo et al. 2004). In the common receiver domain, most likely the primary and noise energy can be separated into different dipping angles by applying normal moveout corrections. However, some complex geologies can make both signal and shear wave noise appear in a very large range of dipping angles, which makes the separation more challenging. The spatial aliasing problem of F-K velocity filtering also needs to be considered during the processing.

In this paper, we propose a new approach that can perform denoising and matching in one step, enhancing wavefield separation. The key point of this method is matching the two components in different dipping angles and frequency panels to separate shear wave noise from signal and promote data sparsity.

Curvelet transform can decompose data into different frequency bands and different dipping angles (Candes et al. 2005) and retain temporal locality. Its sparsity representation of the wave propagation directions and edge preservation makes it a good candidate for shear wave noise attenuation and wavefield separation.

Methodology

Because the shear waves cannot propagate in water, and the conversion from surface wave to P-waves are very limited, we can hardly see any shear wave noise in the hydrophone data. Based on this, we can use hydrophone data to guide geophone data for shear wave attenuation. Assuming that all signals in the geophone data are properly recorded in the hydrophone data, any inconsistent energy between the two components that exists in the hydrophone data is undesired

Shear wave noise attenuation and wavefield separation in curvelet domain

noise. If we can decompose the hydrophone and geophone data into a sparsity promoted domain and compare their local attributes, then we can differentiate the noise and match the obliquity introduced discrepancy simultaneously. Curvelet transform is a good choice for decomposition of data into different frequency bands and dipping angles, thus the signal and noises can be sparsely represented in different curvelet panels.

The first step of the processing workflow is transforming both hydrophone and geophone data into curvelet domain. Since the hydrophone data is shear wave noise free, geophone data will be matched to hydrophone data for noise attenuation purposes. In this step we will match the envelope only to preserve the phase information. Therefore, after attenuation we can combine the hydrophone and geophone data to separate the upgoing and downgoing wavefields. When the energy of the geophone sample is not equal to zero, the amplitude scalars are calculated using the following equation:

$$C(s, d, t, x) = \frac{\sqrt{P(s, d, t, x, \text{real})^2 + P(s, d, t, x, \text{imag})^2}}{\sqrt{Z(s, d, t, x, \text{real})^2 + Z(s, d, t, x, \text{imag})^2}} \quad (1)$$

Here C is the scalar that need to be applied to the geophone data for filtering and matching, s and d are scale and dipping angle in curvelet domain, t and x are time and spatial coordinate. P and Z are curvelet coefficient of the input hydrophone and geophone data, which include real and imaginary parts.

Before applying the scalar to the geophone data, we will further calculate a mute threshold for filtering. As we discussed before, the shear wave noise is much stronger in the geophone data than the hydrophone data. A relatively larger scalar indicates stronger shear wave energy exists in

this region. Thus, we compare the scalar with an adaptive soft threshold for further shear wave energy muting. The mute threshold is calculated using the equation:

$$\mu_{s,d} = w_{user} \times \frac{\hat{\sigma}^2}{\hat{\sigma}_x} \quad (2)$$

Here w_{user} is a percentage weight defined by user, $\hat{\sigma}_x$ is the signal variance that can be estimated using hydrophone data $P_{s,d}$, $\hat{\sigma}$ is noise variance that can be estimated using the robust median estimator (Chang et al. 2000):

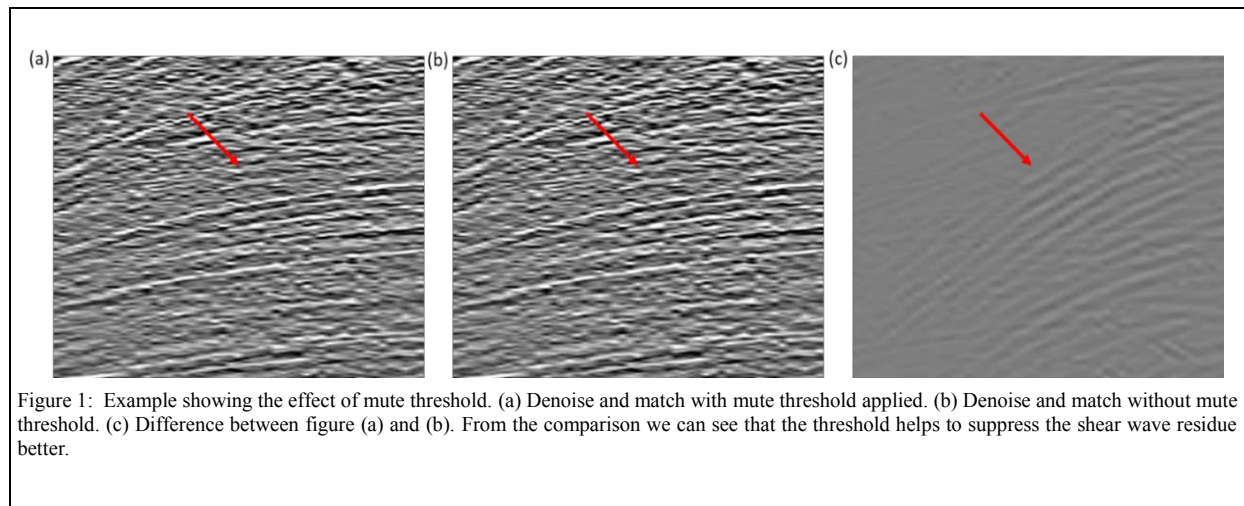
$$\hat{\sigma} = \frac{\text{Median}(|Z_{s,d}|)}{\lambda} \quad (3)$$

λ is a constant value that estimate as 0.6745. Then the previously calculated amplitude scalar will be adjusted accordingly for further shear wave suppression:

$$C_{mute}(s, d, t, x) = \begin{cases} 0 & C(s, d, t, x) < \mu_{s,d} \\ C(s, d, t, x) & C(s, d, t, x) \geq \mu_{s,d} \end{cases} \quad (4)$$

With the threshold being applied, all the filtered scalars will be applied to the geophone curvelet coefficient for noise suppression and amplitude matching. Lastly, we inverse transform the matched geophone data back to time domain.

Figure 1 shows, by applying the mute threshold, the shear wave noise can be suppressed better than with direct envelope matching



Shear wave noise attenuation and wavefield separation in curvelet domain

Examples

The proposed method has been applied on a real ocean bottom node dataset for validation. The dataset used here is Amendment Phase I, which is located in northern Gulf of Mexico (Figure 2). Figure 3 (a) and (b) are one hydrophone and geophone receiver gather before shear wave noise suppression and matching. The red arrow points out the strong shear wave noise in the geophone gather. Figure 3 (c) shows the geophone data after processing. Shear wave noise is significantly attenuated when compared with the input data. We also present the upgoing and downgoing wavefield after P/Z summation in figure 4 (a) and (b), respectively. From the figure we can verify that hydrophone and geophone recordings are well calibrated and coupled, with

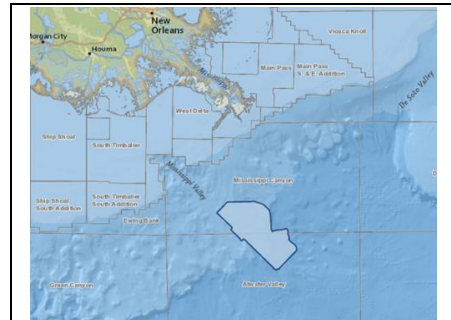


Figure 2. The real data examples used in this abstract is Amendment Phase I located within Gulf of Mexico

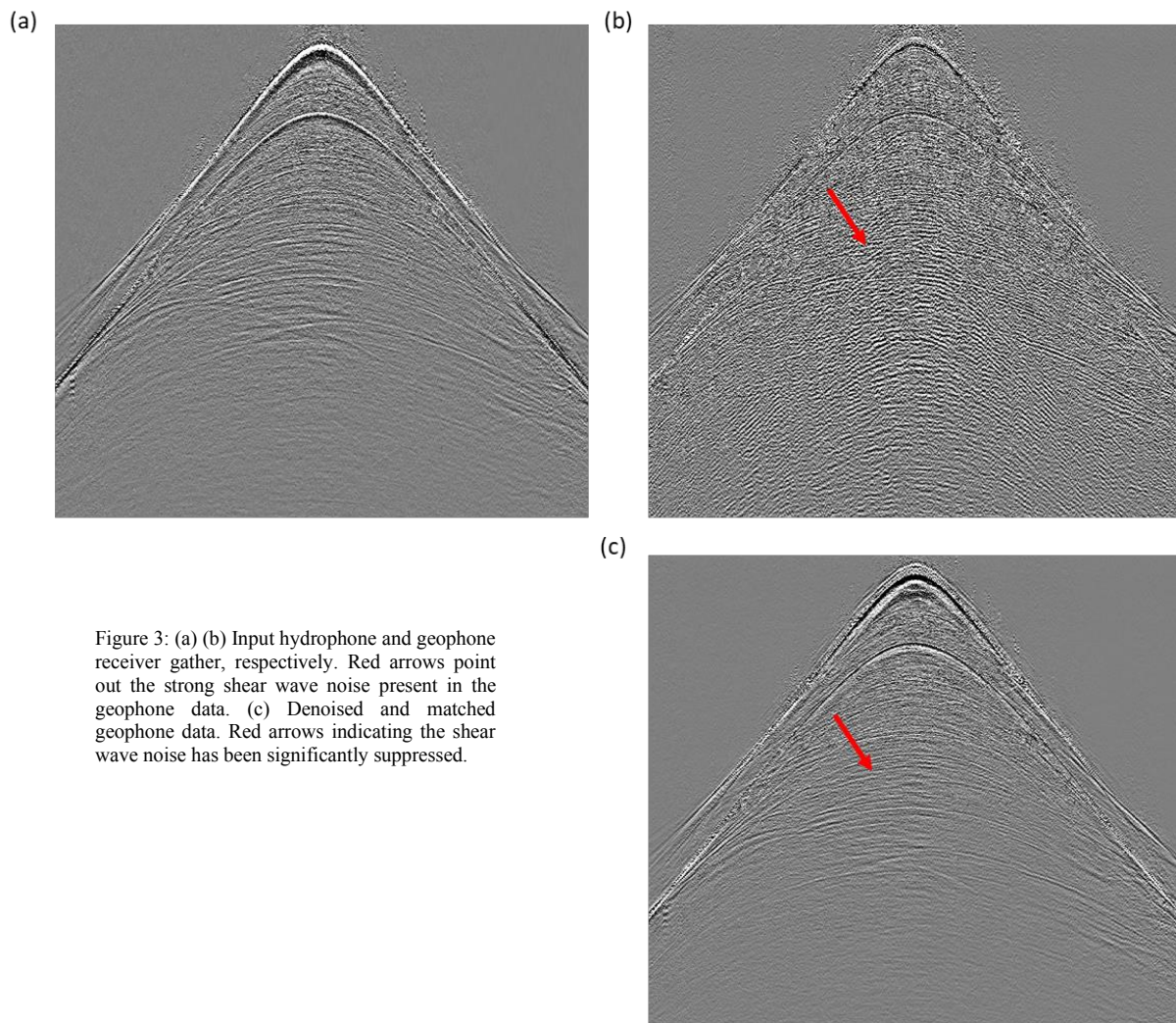


Figure 3: (a) (b) Input hydrophone and geophone receiver gather, respectively. Red arrows point out the strong shear wave noise present in the geophone data. (c) Denoised and matched geophone data. Red arrows indicating the shear wave noise has been significantly suppressed.

Shear wave noise attenuation and wavefield separation in curvelet domain

no obvious upgoing or downgoing residue energy observed in the opposite direction wavefields. Figure 5 shows a single node line RTM image for quality control purposes, where Figure 5 (a) is that using the hydrophone data treated as if it were the upgoing wavefield, and Figure 5 (b) is the image after migrating the separated upgoing wavefield. Wavefield separation successfully improves the image of the upgoing wavefield by removing the downgoing component and increasing the signal to noise ratio, which makes the RTM image much cleaner. Red arrows point out some obvious downgoing residues that overlap with upgoing signals. The proposed method removed these residues and revealed the structures underneath.

Conclusions

In this paper we proposed a new method for ocean bottom seismic data shear wave attenuation and upgoing/downgoing

wavefield separation. By taking advantage of the sparsity promoting property in the curvelet domain, we have developed an integrated workflow to combine the two algorithms. The application to a real data example demonstrates that the new method can effectively suppress shear wave energy and calibrate the geophone data with the hydrophone data in one step, which improves both the efficiency and quality of the upgoing/downgoing wavefield separation.

Acknowledgements

The authors thank TGS, and partner WesternGeco, for the permission to present this work. We also would like to thank our colleagues for generous help and discussions.

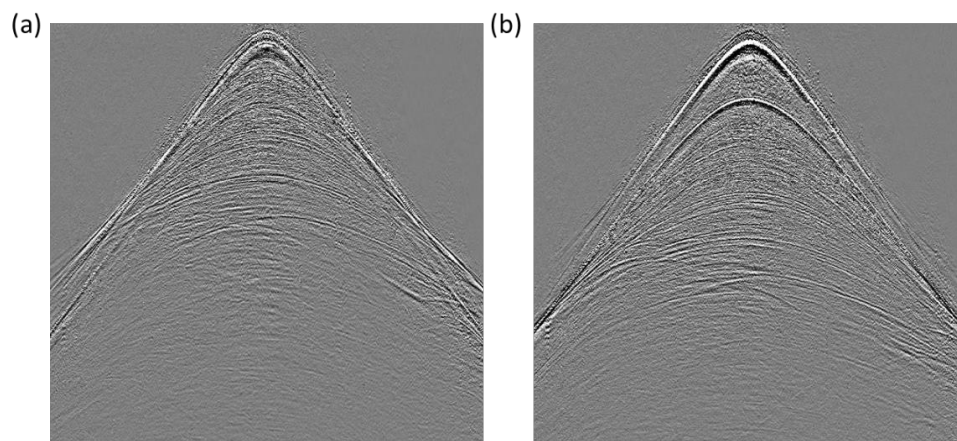


Figure 4: (a) Upgoing wavefield after the proposed processing method. (b) Downgoing wavefield after the proposed processing method.

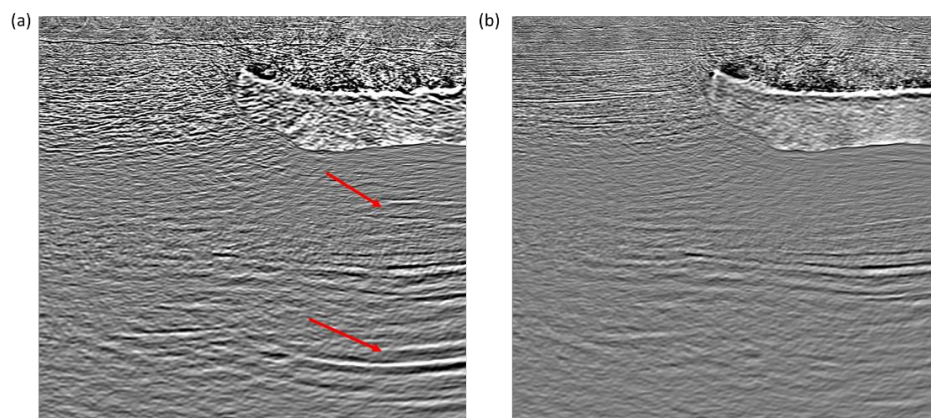


Figure 5: (a) Single node line RTM image using one entire hydrophone data treated as if it has only upgoing energy; (b) Single node line RTM image using the upgoing wavefield processed with the proposed method

REFERENCES

- Brittan, J., and J. Starr, 2003, Applications of adaptive noise attenuation to dual sensor seismic data: 73 rd Annual International Meeting, SEG, Expanded Abstracts, 865–868.
- Candes, E. J., L. Demanet, D. L. Donoho, and L. Ying, 2005, Fast discrete curvelet transforms: California Institute of Technology, Technical Report.
- Chang, S. G., B. Yu, and M. Vetterli, 2000, Adaptive wavelet thresholding for image denoising and compression: IEEE Transactions on Image Processing, **9**, 1532–1546
- Paffenholz, J., P. Docherty, R. Schurteff, and D. Hays, 2006a, Shear wave noise on OBS vz data – Part I: evidence from field data: 68th Conference and Exhibition, EAGE, Extended Abstracts, A071.
- Paffenholz, J., P. Docherty, R. Schurteff, and D. Hays, 2006b, Shear wave noise on OBS vz data – Part II: Elastic modeling of scatters in the seabed: 68th Conference and Exhibition, EAGE, Extended Abstracts, A072.
- Shatilo, A. P., R. E. Duren, and T. Rape, 2004, Effect of noise suppression on quality of 2C OBC image: 74th Annual International Meeting, SEG, Extended Abstracts, 817–920.